JOURNAL OF MATERIALS SCIENCE 25 (1990) 2487–2492

High temperature deformation behaviour of $MoSi_2$ and WSi_2 single crystals

K. KIMURA*, M. NAKAMURA, T. HIRANO
National Research Institute for Metals, Tsukuba Laboratory, Tsukuba, Ibaraki 305, Japan

High temperature deformation behaviour of $MoSi_2$ and WSi_2 single crystals, which both oriented near $\langle 001 \rangle$ and near $\langle 100 \rangle$, have been studied by compression tests over the temperature range of 1100 to 1500° C in a high vacuum of less than 6×10^{-4} Pa. At elevated temperatures, several per cent compression deformation is possible in both $MoSi_2$ and WSi_2. Slips on $\{110\}$ and $\{013\}$ planes, the dislocation with the direction of Burgers vector $\langle 331 \rangle$ and the stacking fault on $\{110\}$ plane are observed in both deformed $MoSi_2$ and WSi_2. In $MoSi_2$, the 0.2% offset stress of the sample oriented $\langle 001 \rangle$ is higher than that of the sample oriented $\langle 100 \rangle$. The higher strength of the sample oriented $\langle 001 \rangle$ is related to the higher CRSS for the main slip plane of it. The reverse orientation dependence of the strength in WSi_2 is also correlated with the difference in CRSS on $\{110\}$ and $\{013\}$ planes, which shows the opposite result to $MoSi_2$. The higher CRSS on $\{110\}$ plane in WSi_2 compared to that on $\{013\}$ may be caused by the formation of a large number of stacking faults on $\{110\}$ plane.

1. Introduction

Recently, many investigations have been reported on the transition metal silicides [1–14]. Most of this research has been focused on the thin films on a silicon substrate, which are used as gate contacts in integrated circuits [1–10, 13, 14]. The high melting point and excellent resistances to oxidation and corrosion of refractory metal silicides mean that they are useful not only for electronic materials, but also for materials at temperatures higher than 1400° C [15]. In particular, $MoSi_2$ is a promising material. Its melting point is 2020° C. In fact, $MoSi_2$ has already been used as a coating material [15]. Recently, there have been a few reports on the mechanical properties of $MoSi_2$ [16, 17]. However, the deformation mechanisms of it have not yet been understood sufficiently. In this investigation, WSi_2 as well as $MoSi_2$ is used, because the melting point of WSi_2, 2164° C, is higher than that of $MoSi_2$ and the crystal structures of both silicides are the same. High temperature compression tests of $MoSi_2$ and WSi_2 were performed over the temperature range 1200 to 1500° C, in order to clarify the high temperature deformation mechanism. Mechanical properties and dislocation substructures are discussed by comparing both silicides.

2. Experimental procedures

2.1. Sample preparation

Single crystals were grown by a floating zone method. The procedure is the same as previously reported [18]. Raw materials for single crystal growth, with a stoichiometric composition, were melted in argon-arc furnaces, using high purity Mo (99.99%), W (99.99%) and Si (99.99%). The growth chamber of the floating zone furnace was evacuated to less than 5×10^{-4} Pa. The single crystals were then grown in high purity argon gas at a flow rate of $2\,l\,min^{-1}$.

Monocrystalline $MoSi_2$ (oriented $\langle 001 \rangle$ and $\langle 100 \rangle$) and WSi_2 (oriented $\langle 001 \rangle$) were grown at a growth rate of $10\,mm\,h^{-1}$, using seed crystals. The grown crystals of $MoSi_2$ and WSi_2 were annealed in a vacuum for 5 h at 1300 and 1350° C, respectively.

2.2. Compression test

The crystal structure of $MoSi_2$ and WSi_2 is tetragonal and belongs to the space group I4/mmm ($C11_b$) and is shown in Fig. 1. The lattice constants of both silicides are quite similar: $a = 0.3202$ nm, $c = 0.7851$ nm for $MoSi_2$ and $a = 0.3211$ nm, $c = 0.7868$ nm for WSi_2. The close packed direction is [0 0 1]. Compression tests were then carried out with the specimens oriented near $\langle 001 \rangle$ and its vertical direction, near $\langle 100 \rangle$, as shown in Fig. 2. The compression test specimens were cut from the annealed single crystals by an electrical discharge machine.

Constant strain-rate compression tests were performed using a Shimadzu Servopulser. Specimens were set between sintered SiC jigs with boron nitride as lubricant. Compression tests were carried out to obtain the 0.2% offset stress and interrupted to observe the substructure. The compression tests were conducted in a vacuum of less than 6×10^{-4} Pa at strain rates of 5×10^{-4} and $5 \times 10^{-5}\,sec^{-1}$ over the temperature ranges of 1100 to 1500° C ($MoSi_2$) and 1200 to 1500° C (WSi_2).

2.3. Transmission electron microscopy

Transmission electron microscopy was used to observe

* *Present address*: Environmental Performance Division, National Research Institute for Metals, 2-3-12 Nakameguro, Meguro, Tokyo 153, Japan.

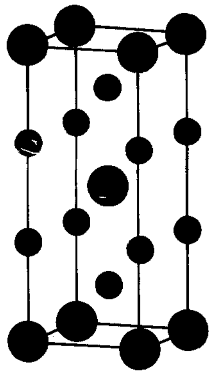

Figure 1 Unit cell of tetragonal $MoSi_2$ and WSi_2 (● molybdenum, tungsten, • silicon).

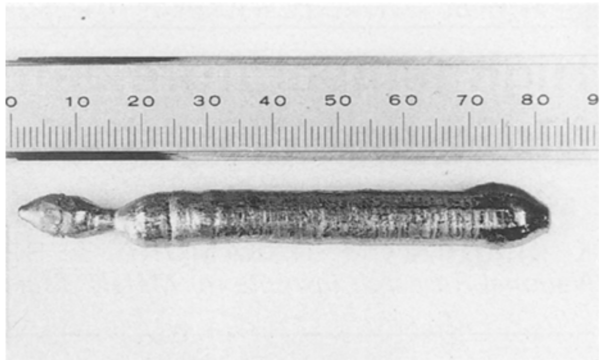

Figure 3 The appearance of WSi_2 single crystal grown by the floating zone method.

the substructures of the compression tested specimens. The discs, 3 mm in diameter and 1 mm in thickness, were cut from those samples by the electrical discharge machine. After reducing the thickness to approximately 100 μm by grinding uniformly, the thickness at the centre of the discs was reduced to about 30 μm by a dimple grinder. Finally, the discs were thinned by ion-beam milling and subjected to transmission electron microscopy. A JEOL 200CX microscope was used at accelerating voltage of 200 kV.

3. Results and discussion

3.1. Single crystal preparation

The appearance of a WSi_2 single crystal grown by the floating zone method is shown in Fig. 3. The shape of $MoSi_2$ single crystals is also the same. The single crystals used in this investigation were approximately 8 mm in diameter.

Very small dislocations were observed in both as-grown silicides by transmission electron microscopy. The single crystals grown by this floating zone method are considered to be of good quality.

3.2. Compression test at elevated temperature

Stress–strain curves of $MoSi_2$ at a strain rate of $5 \times 10^{-4}\,sec^{-1}$ and in the temperature range of 1300 to 1500° C are shown in Fig. 4. The compression tests were interrupted at the end of each curve. The 0.2% offset stresses of M[0 0 1] are higher than those of M[1 0 0] at all temperatures studied. The 0.2% offset stress decreases with an increase in temperature, and the tendency of a decrease in strength is similar in both samples M[0 0 1] and M[1 0 0], irrespective of orientation.

Results on WSi_2 at a strain rate of $5 \times 10^{-5}\,sec^{-1}$ and at the same temperatures as Fig. 4 are shown in Fig. 5. The 0.2% offset stresses of W[1 0 0] are higher than those of W[0 0 1]. This orientation dependence of the strength in WSi_2 is the opposite to the case in $MoSi_2$. The 0.2% offset stress of W[0 0 1] decreases with an increase in temperature, as well as in both M[0 0 1] and M[1 0 0]. In sample W[1 0 0], however, the extent of a decrease in strength with an increase in temperature is very little.

Changes in the 0.2% offset stress of $MoSi_2$ single crystal with temperature are shown in Fig. 6. As for the sample M[0 0 1], the data were not obtained below 1200° C because of pre-yield fracture. Orientation dependence of the 0.2% offset stress is distinctly observed: the 0.2% offset stress of sample M[0 0 1] is higher than that of sample M[1 0 0]. The strength of sample M[0 0 1] is twice that of sample M[1 0 0] at 1300° C and the strain rate of $5 \times 10^{-4}\,sec^{-1}$. Such an orientation dependence of the strength, however, reduces with an increase in temperature and almost disappears at 1500° C.

The strain rate dependence of the strength was examined on sample M[1 0 0]. There is a loss of approximately 100 MPa in 0.2% offset stress with a decrease in strain rate from 5×10^{-4} to $5 \times 10^{-5}\,sec^{-1}$ over the temperature range of 1100 to 1500° C. Although the ductility was never measured quantitatively, compressive deformation of more than 5% is possible in sample M[1 0 0] at the strain rate of $5 \times 10^{-5}\,sec^{-1}$ and 1500° C.

The results on WSi_2 are shown in Fig. 7. The asterisked plots refer to the data which were affected by cracking. Almost the same strain rate dependence of

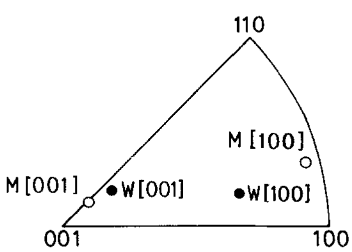

Figure 2 Orientations of the samples used for compression test (○ $MoSi_2$, ● WSi_2).

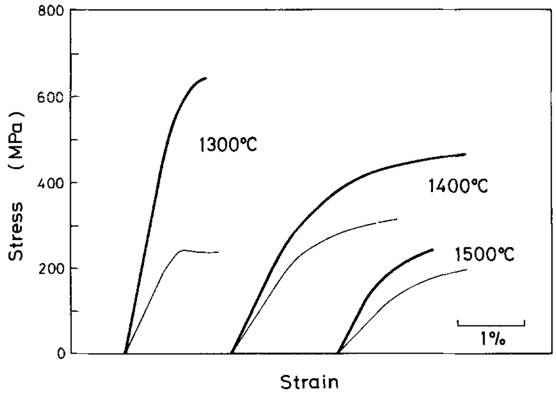

Figure 4 Stress–strain curves of $MoSi_2$ at a strain rate of $5 \times 10^{-4}\,sec^{-1}$ and in the temperature range of 1300 to 1500° C (**—** M[0 0 1], — M[1 0 0]).

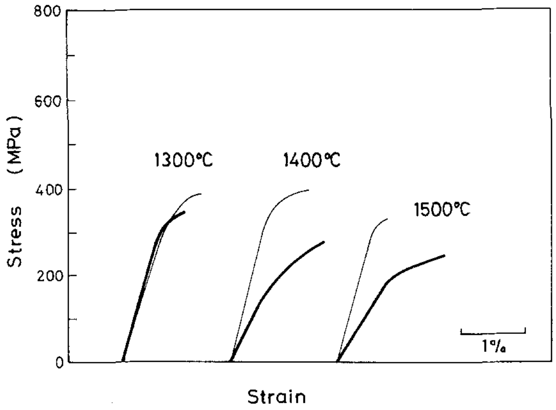

Figure 5 Stress-strain curves of WSi_2 at a strain rate of 5×10^{-5} sec^{-1} and in the temperature range of 1300 to 1500°C (—— W[0 0 1], — W[1 0 0]).

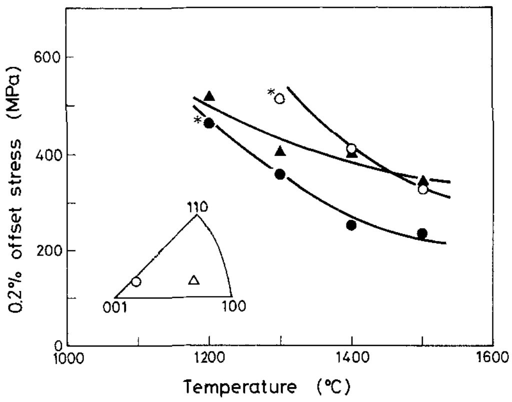

Figure 7 Changes in the 0.2% offset stresses of WSi_2 single crystal with temperature (○ W[0 0 1], strain rate 5×10^{-4} sec^{-1}; ● W[0 0 1], strain rate 5×10^{-5} sec^{-1}; ▲ W[1 0 0], strain rate 5×10^{-5} sec^{-1}; * crack).

the strength, as in sample M[1 0 0], is observed in sample W[0 0 1]. However, the orientation dependence of the strength in WSi_2 is completely opposite to that in $MoSi_2$. The 0.2% offset stress of sample W[1 0 0] is larger than that of sample W[0 0 1], contrary to the case in $MoSi_2$. Moreover, the extent of such an orientation dependence of the strength increases with an increase in temperature from 1200 to 1500°C. Ductility of WSi_2 was considerably lower than that of $MoSi_2$. Results of slip trace analysis on the deformed specimens are summarized in Table I. In both samples M[1 0 0] and W[1 0 0], the slip plane is {1 1 0}, which is the close-packed plane in $C11_b$ structure. In sample M[0 0 1], the main slip plane is {0 1 3}, although slip on {1 1 0} plane is also observed. On the other hand, in sample W[0 0 1], the slip plane is only {0 1 3}, and small {1 1 0} slips are observed.

3.3. Transmission electron microscopy

Dark field transmission electron images of the samples M[0 0 1], deformed by 0.4% at 1300°C and 5×10^{-4} sec^{-1}, and M[1 0 0], deformed by 3.8% at 1400°C and 5×10^{-4} sec^{-1}, are shown in Figs 8 and 9, respectively. In both samples, a great number of dislocations are introduced by the compressive deformation at the elevated temperatures. Almost all dislocations have a Burgers vector with the direction of ⟨3 3 1⟩ in both

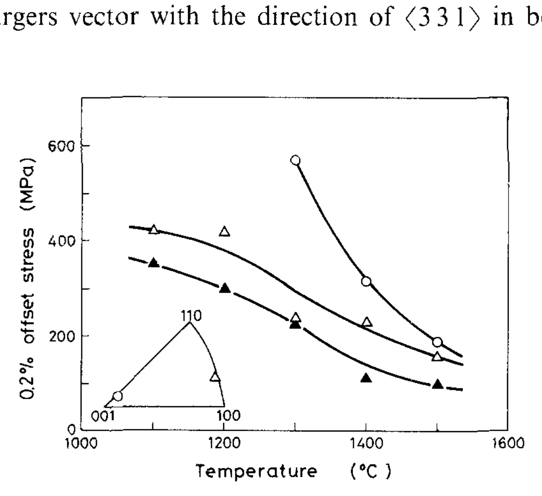

Figure 6 Changes in the 0.2% offset stresses of $MoSi_2$ single crystal with temperature (○ M[0 0 1], strain rate 5×10^{-4} sec^{-1}, △ M[1 0 0], strain rate 5×10^{-4} sec^{-1}; ▲ M[1 0 0], strain rate 5×10^{-5} sec^{-1}).

samples. Then, it is ascertained that the slips occur along ⟨3 3 1⟩ direction on both {1 1 0} and {0 1 3} planes, which is the same as reported by Umakoshi *et al.* [16]. The dislocation density of sample M[0 0 1] (Fig. 8), which shows higher 0.2% offset stress, is higher than that of M[1 0 0] (Fig. 9). Moreover, the fringe contrast due to stacking fault is observed only in sample M[1 0 0] (Fig. 9).

Bright field images, taken from the identical area of the same sample as Fig. 9, using three different reflections (a) $g = \bar{1}\,0\,\bar{3}$, (b) $g = \bar{1}\,\bar{1}\,0$ and (c) $g = 0\,0\,6$, are shown in Fig. 10. The fringe contrast of the stacking fault, which is visible in (a) $g = \bar{1}\,0\,\bar{3}$, is invisible in both (b) $g = \bar{1}\,\bar{1}\,0$ and (c) $g = 0\,0\,6$. Therefore, the stacking fault is formed on a {1 1 0} plane, which is the close-packed plane of $C11_b$ structure.

The dark field image of sample W[0 0 1], deformed by 1.6% at 1400°C and 5×10^{-5} sec^{-1}, and the bright field image of sample W[1 0 0], deformed by 0.3% at 1500°C and 5×10^{-5} sec^{-1}, are shown in Figs 11 and 12, respectively. A large number of dislocations are introduced, especially in sample W[0 0 1]. The dislocation density in sample W[0 0 1] is much higher than those in both $MoSi_2$ (Figs 8 and 9). Almost all dislocations have a Burgers vector with the direction of ⟨3 3 1⟩, similar to that of $MoSi_2$. A large amount of fringe contrast due to stacking fault are observed in both W[0 0 1] and W[1 0 0], and the quantities of the stacking fault are significantly larger than that in $MoSi_2$ (Fig. 9). Those stacking faults are also formed on {1 1 0} planes similar to those of $MoSi_2$.

3.4. Stacking fault in $C11_b$ structure

A characteristic point in the deformed microstructures is the formation of stacking faults on the {1 1 0} plane, as mentioned above. In this section, the for-

TABLE I Slip planes of the samples obtained by slip trace analysis

Sample		Slip plane
$MoSi_2$	M[0 0 1]	{0 1 3}, {1 1 0}
	M[1 0 0]	{1 1 0}
WSi_2	W[0 0 1]	{0 1 3}
	W[1 0 0]	{1 1 0}

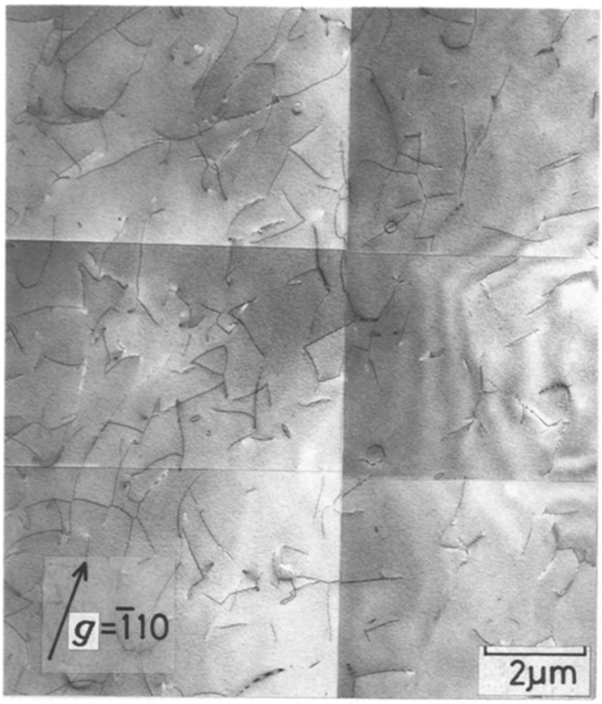

Figure 8 Dark field transmission electron image of the sample M[0 0 1] deformed by 0.4% at 1300° C and $5 \times 10^{-4}\,sec^{-1}$.

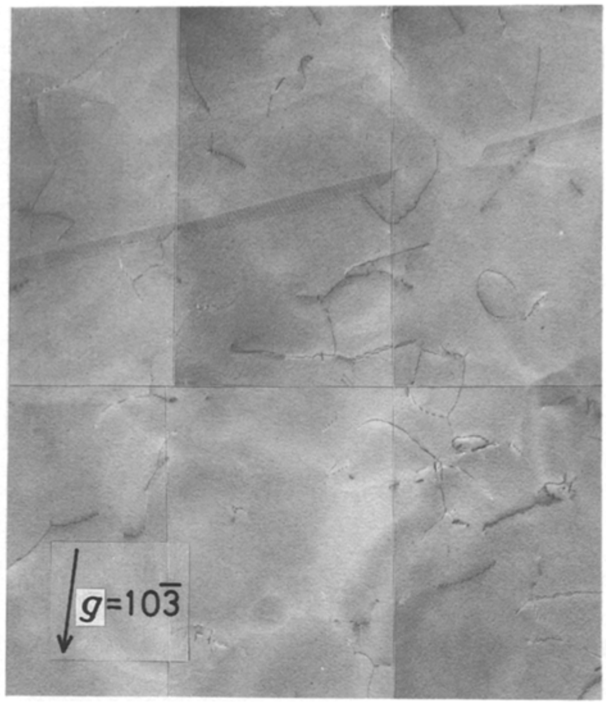

Figure 9 Dark field transmission electron image of the sample M[1 0 0] deformed by 3.8% at 1400° C and $5 \times 10^{-4}\,sec^{-1}$.

mation of a stacking fault in $MoSi_2$ and WSi_2 is discussed.

A close-packed plane of $MoSi_2$ and WSi_2 is {1 1 0} and the atom configuration of this plane is shown in Fig. 13a. A molybdenum or tungsten atom is located at the centre of a hexagonal cell which consists of silicon atoms. The stacking order of {1 1 0} planes is ABABAB in the same way as h c p metal, as shown in Fig. 13b.

It has been reported that in $C11_b$ type $MoSi_2$ phase transition to β-$MoSi_2$ takes place above 1900° C [19]. β-$MoSi_2$ is hexagonal, and belongs to the space group $P6_222$ (C40) with $a = 0.4642$ nm and $c = 0.6529$ nm. On the contrary, low temperature phases of $MoSi_2$ and WSi_2, which are the same hexagonal structure as β-$MoSi_2$, have been reported below about 550° C, though they are restricted to thin films on the silicon substrate [1, 4–9, 13, 14]. The atomic configuration on the close-packed plane of C40 structure is the same as that of $C11_b$ structure. The difference between $C11_b$ and C40 structures is only the stacking order: ABABAB in $C11_b$ and ABCABC in C40, as shown in Figs 13b and 13c, respectively. Therefore, $C11_b$ and C40 are considered to be crystallographically and thermodynamically similar to each other, although it is not always clear which is the stable low temperature phase. The stacking order of the C40 structure is easily obtained from $C11_b$ structure by slip along the ⟨1 1 1⟩

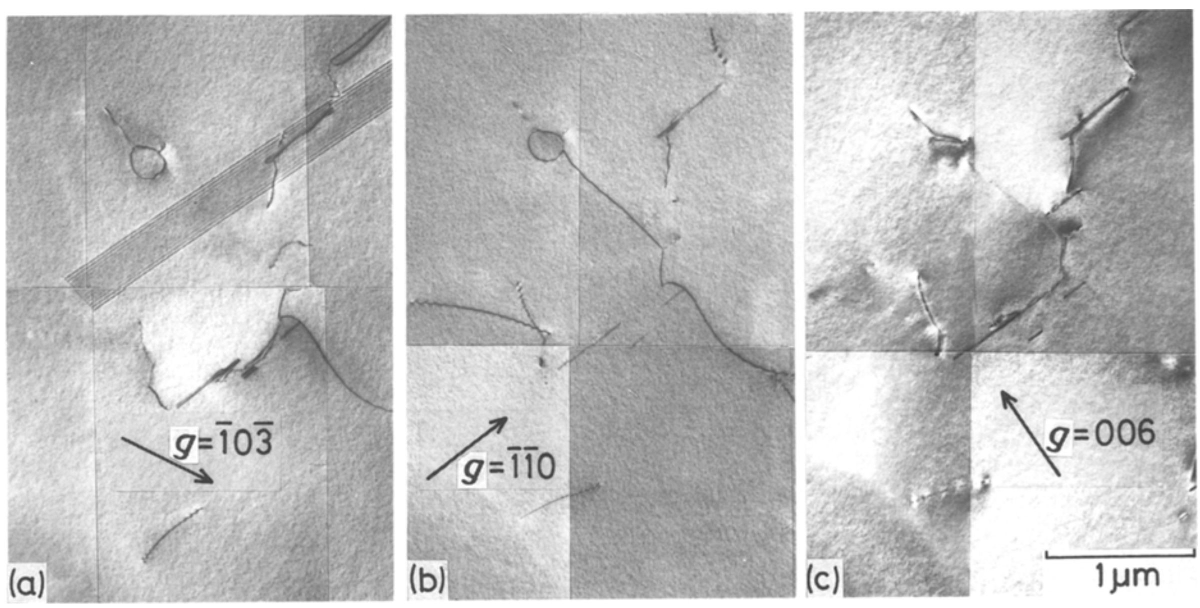

Figure 10 Bright field transmission electron images taken from the identical area of the sample M[1 0 0] deformed by 3.8% at 1400° C and $5 \times 10^{-4}\,sec^{-1}$, using three different reflections (a) $g = \bar{1}0\bar{3}$, (b) $g = \bar{1}\bar{1}0$ and (c) $g = 006$.

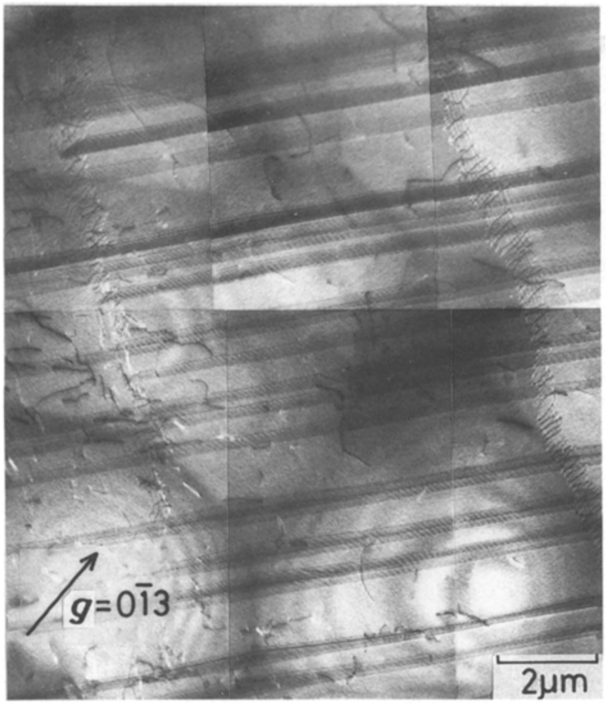

Figure 11 Dark field transmission electron image of the sample W[0 0 1] deformed by 1.6% at 1400°C and 5×10^{-5} sec^{-1}.

direction on the close-packed plane of {1 1 0}. Then, the stacking order of ABC is formed locally at the stacking fault.

3.5. Critical resolved shear stress

The highest Schmid factors for the slip systems of {0 1 3}⟨3 3 1⟩ in M[0 0 1] and {1 1 0}⟨3 3 1⟩ in M[1 0 0] are 0.454 for (0 1 3)[$\bar{3}$ $\bar{3}$ 1] in M[0 0 1] and 0.418 for (1 1 0)[3 $\bar{3}$ 1] in M[1 0 0], respectively. By using these values, the critical resolved shear stresses (CRSS) for {1 1 0}⟨3 3 1⟩ and {0 1 3}⟨3 3 1⟩ of $MoSi_2$ are cal-

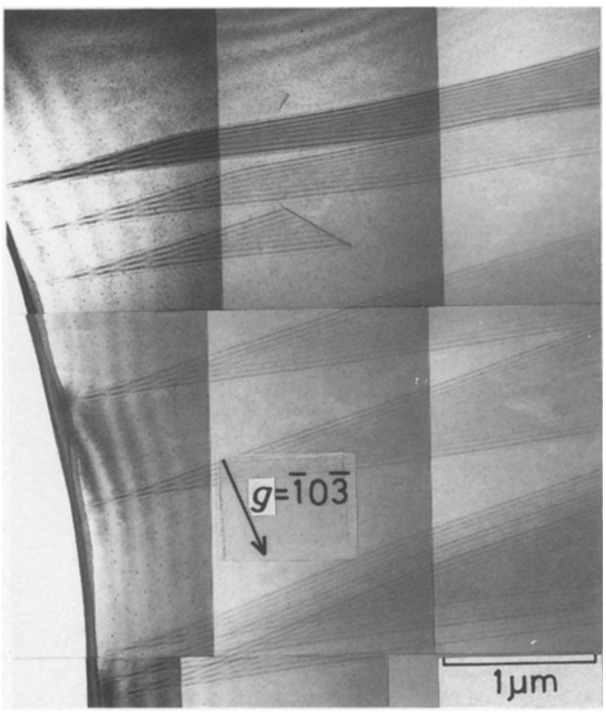

Figure 12 Bright field transmission electron image of the sample W[1 0 0] deformed by 0.3% at 1500°C and 5×10^{-5} sec^{-1}.

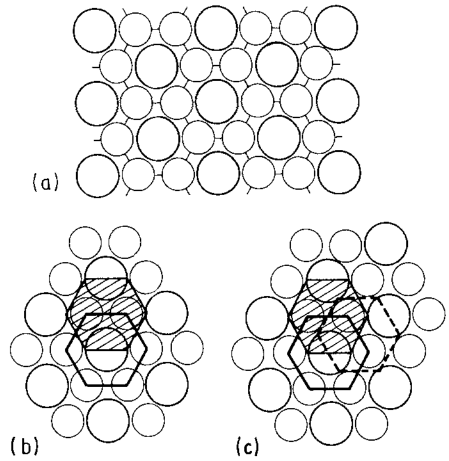

Figure 13 (a) The atom configuration of {1 1 0} plane, which is a close-packed one, of $MoSi_2$. (b) The stacking order of a close-packed plane in tetragonal ($C11_b$) $MoSi_2$ and WSi_2. (c) The stacking order of a close-packed plane in hexagonal (C40) $MoSi_2$ and WSi_2. (○ molybdenum, tungsten, ○ silicon, ◯ A, ◍ B, ◌ C).

culated, and shown in Fig. 14. The data reported by Umakoshi *et al.* are also plotted in the same figure. The CRSS on {0 1 3} is much higher than that on {1 1 0}. The main slip planes of samples M[0 0 1] and M[1 0 0] are {0 1 3} and {1 1 0}, respectively, as shown in Table I. Therefore, the higher strength and dislocation density of sample M[0 0 1] are in agreement with the higher CRSS for main slip plane of it.

CRSS of WSi_2 are shown in Fig. 15. CRSS on {1 1 0} is much higher than that on {0 1 3}, contrary to $MoSi_2$. The difference in CRSS corresponds to the orientation dependence of the 0.2% offset stress. Higher CRSS on {1 1 0} should be correlated to the formation of a large number of stacking faults on the {1 1 0} plane. It is considered that, therefore, the differences in orientation dependence on the strength of $MoSi_2$ and WSi_2 at elevated temperatures may be essentially correlated with the difference in the formation of stacking faults. Further research is, of course, needed to clarify these points.

4. Summary

The deformation behaviours of $MoSi_2$ and WSi_2 single crystals, which are oriented both near ⟨0 0 1⟩ and near

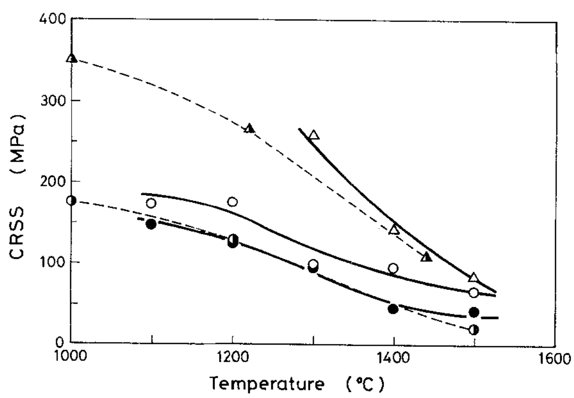

Figure 14 Changes in CRSS for {1 1 0} ⟨3 3 1⟩ and {0 1 3} ⟨3 3 1⟩ of $MoSi_2$ with temperature (○ {1 1 0} ⟨3 3 1⟩, 5×10^{-4} sec^{-1}; △ {0 1 3} ⟨3 3 1⟩, 5×10^{-4} sec^{-1}; ● {1 1 0} ⟨3 3 1⟩, 5×10^{-5} sec^{-1}; ◑ {1 1 0} ⟨3 3 1⟩, Umakoshi *et al.*; ▲ {0 1 3} ⟨3 3 1⟩, Umakoshi *et al.*).

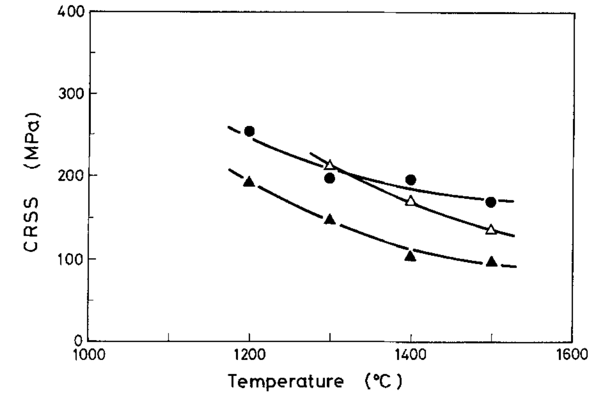

Figure 15 Changes in CRSS for {1 1 0} ⟨3 3 1⟩ and {0 1 3} ⟨3 3 1⟩ of WSi_2 with temperature (△ {0 1 3} ⟨3 3 1⟩, 5×10^{-4} sec^{-1}; ● {1 1 0} ⟨3 3 1⟩, 5×10^{-5} sec^{-1}; ▲ {0 1 3} ⟨3 3 1⟩, 5×10^{-5} sec^{-1}).

⟨1 0 0⟩, have been studied by compression tests using a strain rate of 5×10^{-4} and 5×10^{-5} sec^{-1} over the temperature range of 1100 to 1500° C in a high vacuum of less than 6×10^{-4} Pa.

At elevated temperatures above 1000° C, several per cent compression deformation is possible in both $MoSi_2$ and WSi_2, though the ductility of WSi_2 is relatively inferior to that of $MoSi_2$. With an increase in temperature, the 0.2% offset stresses of the samples M[0 0 1], M[1 0 0] and W[0 0 1] decreased. Only in sample W[1 0 0], however, is the extent of the decrease in strength with an increase in temperature very small. In $MoSi_2$, the 0.2% offset stress of sample M[0 0 1] is higher than that of sample M[1 0 0]. For WSi_2, on the other hand, the orientation dependence of the strength is opposed to that for $MoSi_2$, the 0.2% offset stress of sample W[1 0 0] is higher than that of sample W[0 0 1].

Slips on the {1 1 0} plane, which is a close-packed plane, and on the {0 1 3} plane are observed. The dislocations with the direction of Burgers vector ⟨3 3 1⟩, and the stacking fault on the {1 1 0} plane are introduced by high temperature deformation in both $MoSi_2$ and WSi_2. In $MoSi_2$, the dislocation density of the sample M[0 0 1], which shows higher strength, is higher than that of sample M[1 0 0]. The amount of stacking faults in WSi_2 is significantly greater than for $MoSi_2$.

In $MoSi_2$, CRSS on {0 1 3} plane is much higher than that on {1 1 0} plane. The higher 0.2% offset stress and the dislocation density of the sample M[0 0 1] are correlated with the higher CRSS for main slip plane, {1 1 0}, of it. The reverse orientation dependences of strength and dislocation density in WSi_2 are also correlated with the difference in CRSS on {1 1 0} and {0 1 3} planes, which shows the opposite result to $MoSi_2$. Finally, it is considered that the higher CRSS on {1 1 0} plane in WSi_2 might be caused by the formation of a large number of stacking faults.

References

1. A. GUIVARC'H, P. AUVRAY, L. BERTHOU, M. LE CUN, J. P. BOULET, P. HENOC, G. PELOUS and A. MARTINEZ *J. Appl. Phys.* **49** (1978) 233.
2. S. ZIRINSKY, W. HAMMER, F. D'HEURLE and J. BAGLIN, *Appl. Phys. Lett.* **33** (1978) 76.
3. J. BAGLIN, F. D'HEURLE and S. PETERSSON, *ibid.* **33** (1978) 289.
4. J. BAGLIN, J. DEMPSEY, W. HAMMER, F. D'HEURLE, S. PETERSSON and C. SERRANO, *J. Electron. Mater.* **8** (1979) 641.
5. M. Y. TSAI, C. S. PETERSSON, F. M. D'HEURLE and V. MANISCALCO, *Appl. Phys. Lett.* **37** (1980) 295.
6. F. M. D'HEURLE, C. S. PETERSSON and M. Y. TSAI, *J. Appl. Phys.* **51** (1980) 5976.
7. S. P. MURARKA, M. H. READ and C. C. CHANG, *ibid.* **52** (1981) 7450.
8. K. SHIBATA, S. SHIMA and M. KASHIWAGI, *J. Electrochem. Soc.* **129** (1982) 1527.
9. G. BOMCHIL, D. BENSAHEL, A. GOLANSKI, F. FERRIEU, G. AUVERT, A. PERIO and J. C. PFISTER, *Appl. Phys. Lett.* **41** (1982) 46.
10. A. PERIO, J. TORRES, G. BOMCHIL, F. ARNAUD D'AVITAYA and R. PANTEL, *ibid.* **45** (1984) 857.
11. PH. GED, R. MADAR and J. P. SENATEUR, *Phys. Rev. B* **29** (1984) 6981.
12. O. THOMAS, J. P. SENATEUR, R. MADAR, O. LABORDE and E. ROSENCHER, *Solid State Commun.* **55** (1985) 629.
13. W. T. LIN and L. J. CHEN, *Appl. Phys. Lett.* **46** (1985) 1061.
14. F. M. D'HEURLE, F. K. LEGOUES and R. JOSHI, *ibid.* **48** (1986) 332.
15. S. M. TUOMINEN and J. M. DAHL, *J. Less-Common Met.* **81** (1981) 249.
16. Y. UMAKOSHI, T. HIRANO, T. SAKAGAMI and T. YAMANE, *Scripta Metall.* **23** (1989) 87.
17. Y. UMAKOSHI, T. SAKAGAMI, T. YAMANE and T. HIRANO *Phil. Mag. Lett. A* **59** (1989) 159.
18. H. TABATA and T. HIRANO, *J. Jpn Inst. Met.* **52** (1988) 1154.
19. V. N. SVECHNIKOV, YU. A. KOCHERZHINSKII and L. M. YUPKO, *DAN Ukr SSR A* **6** (1970) 553.

Received 20 March
and accepted 4 September 1989